Structural Chemistry (2023) 34:1927–1934
https://doi.org/10.1007/s11224-023-02210-3

RESEARCH

Synthesis, NoSpherA2 refinement, and noncovalent bonding of abiraterone bromide monohydrate

Alexander A. Korlyukov[1] · Petr A. Buikin[1,2] · Pavel V. Dorovatovskii[3] · Anna V. Vologzhanina[1]

Received: 4 July 2023 / Accepted: 20 July 2023 / Published online: 3 August 2023

Abstract

Abiraterone (AbirOH) is an active metabolite of abiraterone acetate (AbirAc) used as a therapeutic agent against prostate cancer. A variety of its solid forms includes polymorphs of pure abiraterone, abiraterone acetate, and cocrystals of abiraterone acetate with carboxylic acids, and a pyridinium-containing $(HAbirOH)^+$ salt as well. Herein, we present the crystal structure of $(HAbirOH)Br \cdot H_2O$ as obtained by means of NoSpherA2 refinement applied to reveal charge density distribution for abiraterone from routine single-crystal X-ray diffraction experiment. Peculiarities of noncovalent interactions in this salt are discussed in terms of molecular Voronoi and Hirshfeld surfaces. The AbirOH packing in this salt and in previously reported solids is analyzed by means of the "Crystal Packing Similarity" tool.

Keywords Abiraterone · Active pharmaceutical ingredient · Crystal Packing Similarity · Hirshfeld molecular surface · NoSphereA2 refinement · Single-crystal X-ray diffraction · Voronoi molecular surface

Introduction

Abiraterone (AbirOH) is an active metabolite of the commercially available drug *Zytiga* (abiraterone acetate, AbirAc) used to treat prostate cancer. According to the results provided by macromolecular crystallography, nitrogen atom can coordinate heme fragment of androgen receptors. A detailed study of the ligand-receptor binding that was carried out on the base of combined study utilizing experimental charge density and Voronoi tessellation [1] as main methods has shown that weak hydrophobic H…H interactions between steroid fragment and amino acid residues are also very important for retention of abiraterone in cavity of receptor formed by peptide chains and heme fragment. Mainly the hydrophobic molecular surface of AbirAc results in its poor solubility; thus, by cocrystallization of AbirAc with some coformers, novel solid forms of AbirAc with enhanced solubility were obtained [2, 3]. Acidic media hydrolysis of AbirAc [4] and protonation of the pyridine moiety can easily occur, which also allows to afford new solid forms of abiraterone for pharmaceutics [5]. Herein, we present the structure of $(HAbirOH)Br \cdot H_2O$ (17-(pyridinium-3-yl) androsta-5,16-dien-3-ol bromide monohydrate, **1**; Scheme 1) that was found to be isostructural with previously studied chloride-containing analog [5].

Solid $(HAbirOH)Cl \cdot H_2O$ and $(HAbirOH)Br \cdot H_2O$ give an opportunity to obtain charge distribution in the region of abiraterone that can be of interest for biochemists. However, the chloride-containing salt was investigated at 298 and 100 K [5, 6] using a standard independent atom model only. We also failed to obtain a single crystal of the bromide-containing analog suitable for high-resolution X-ray diffraction experiment. Nevertheless, data collected by us allow application of aspherical structure factors [7] to obtain wavefunction related to unique parts of the unit cell. This

✉ Anna V. Vologzhanina
vologzhanina@mail.ru

Alexander A. Korlyukov
alex@xrlab.ineos.ac.ru

Petr A. Buikin
peterzzz@mail.ru

Pavel V. Dorovatovskii
paulgemini@mail.ru

[1] A. N. Nesmeyanov Institute of Organoelement Compounds, Russian Academy of Sciences, 28 Vavilov St., Moscow 119334, Russia

[2] N. S. Kurnakov Institute of General and Inorganic Chemistry, Russian Academy of Sciences, 31 Leninskii Prosp., Moscow 119991, Russia

[3] National Research Center "Kurchatov Institute", 1 Kurchatova pl., Moscow 123098, Russia

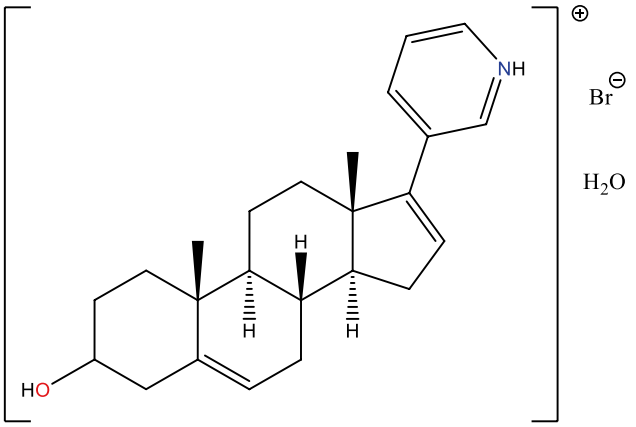

Scheme 1 Schematic representation of 17-(pyridinium-3-yl)androsta-5,16-dien-3-ol bromide monohydrate

approach is suitable for the evaluation of many properties of small molecules and their solids, for instance, low-frequency lattice vibrations [8], charge density and NCI analysis [9, 10], and proton migration study of strong H-bonds [11]. To our knowledge, data about charge distribution in solids of active pharmaceutical ingredients obtained by means of the NoSphereA2 refinement are limited by recent work concerning crystal structure of pure imatinib [12].

Experimental

Solution of abiraterone acetate (0.012 g, 0.05 mmol) in 1 ml of ethanol was added to a solution of $FeBr_3$ (0.087 g, 0.5 mmol) in 2 ml of ethanol. Mixture was heated and solution was cooled on air. After 2 days of standing at RT, white precipitate formed. Single crystals of $C_{24}H_{34}BrNO_2$ were obtained from this precipitate. ^1H and ^{13}C NMR spectra were recorded on 400 MHz and 101 spectrometers in DMSO-d_6 solution. The powder X-ray diffraction patterns were obtained in reflection mode. The measurements were performed with a Bruker D8 Advance diffractometer (Bragg–Brentano geometry) equipped with motorized slits and a LynxEye 1D position-sensitive detector (CuKa, Ni-filter) in the range $2\Omega = 3–50°$. FTIR spectra were recorded on a Perkin Elmer Spectrum 65 spectrometer in the range of 400–4000 cm^{-1}.

^1H NMR (400 MHz, DMSO-d_6) δ: 0.92–1.08 (m, 2H, CH), 0.99 (s, 3H, CH_3), 1.03 (s, 3H, CH_3), 1.27–2.34 (m, 18H, other CH and CH_2), 3.19–3.31 (m (seems like quintet, J = 5.3 Hz), 1H, CH(OH)), 4.30 (ws, OH, H+, H_2O), 5.30 (d, J = 5.0 Hz, 1H, CH = C), 6.46 (s, 1H, CH = C), 7.93 (t, J = 7.0 Hz, 1H, Ar), 8.49 (d, J = 8.2 Hz, 1H, Ar), 8.73 (d, J = 5.6 Hz, 1H, Ar), 8.86 (s, 1H, Ar). ^{13}C NMR (101 MHz, DMSO-d_6) δ: 16.39, 19.53, 20.80, 30.32, 31.33, 31.84, 32.03, 34.47, 36.71, 37.29, 42.68, 47.15, 50.17, 57.45, 70.42, 120.58, 127.05, 134.33, 135.36, 140.48, 141.37, 141.75, 142.10, 148.74. IR-spectrum (FTIR) (cm^{-1}): 3328 s, 2960 m, 2909 s, 2889 s, 1550 s, 1057 s, 804 s, 684 s.

The intensities of 10,124 reflections were collected at "Belok/XSA" beamline of the Kurchatov Synchrotron Radiation Source [13, 14]. Diffraction patterns were collected using a 1-axis MarDTB goniometer equipped with a Rayonix SX165 CCD 2D positional sensitive CCD detector ($\lambda = 0.745$ Å, φ-scanning in 1.0° steps) in the direct geometry with a detector plane perpendicular to its beam. Approximately 180 diffraction frames were collected for each data set. Thus, obtained data were indexed and integrated using the XDS software suite [15]. At 100 K, crystal system is monoclinic, space group $P2_1$: $a = 6.6520(13)$, $b = 11.136(2)$, $c = 14.513(3)$ Å, $\alpha = 90$, $\beta = 94.25(3)$, $\gamma = 90°$, $V = 1072.1(4)$ $Å^3$, $Z = 2$, $\mu = 2.178$ mm^{-1}, $D_{calc} = 1.389$ g cm^{-3}, $F(000) = 471.2$.

The structure was solved by the dual-space algorithm [16] and initially refined by full-matrix least squares against F^2 using the IAM model (SHELXL program [17]) to $R_1 = 0.0376$ and $wR_2 = 0.0949$, $\rho_{min}/\rho_{max} = -0.93/0.87$ e. Non-hydrogen atoms were refined in an anisotropic approximation; anharmonic refinement for bromine atom was applied. Hydrogen atoms were located on difference Fourier maps and refined with unfixed bond distances; their ADPs were calculated with SHADE3 [18] and fixed at the calculated values. The application of the NoSpherA2 algorithm [7] implemented within the Olex2 package [19] for subsequent refinement led to a noticeable decrease of residual factors. Refinement converged to $R_1 = 0.0295$ (for 5468 observed reflections and 382 parameters), $wR_2 = 0.0693$, and GOF = 1.039 (for 5852 independent reflections, $R_{int} = 0.0338$), $\rho_{min}/\rho_{max} = -0.31/0.51$ e.

Peculiarities of the Voronoi molecular polyhedra were calculated using the ToposPro package [20]. The Hirshfeld surface analysis was performed by the CrystalExplorer 17.5 package [21]. Analysis of electron density function and visualization of results were carried out with Multiwfn [22] and VMD software [23].

Results and discussion

In our study of novel solid forms of known active pharmaceutical ingredients [12, 24], the ability of abiraterone acetate to form salts with various metals was examined. Solution of abiraterone acetate in ethanol was added to a solution of $FeBr_3$ in equimolar ratio (1:1). After several days of standing on air at RT, red precipitate formed.

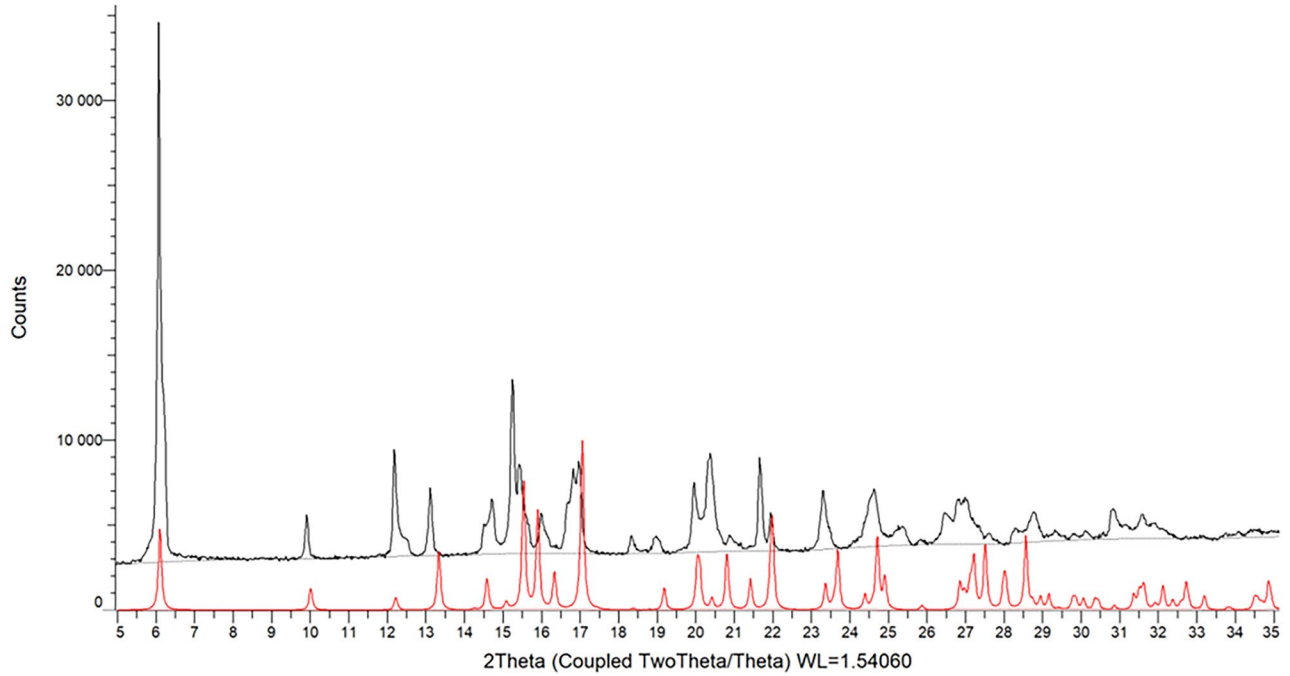

Fig. 1 PXRD patterns of (HAbirOH)Br · H_2O at RT (red line—calculated profile; black line—experimental profile) in 2Ω range 5 − 35°

The red color of precipitate can be easily explained by the formation of colloid $Fe(OH)_3$. At the same time, small colorless crystals were also found in a microscopic study. The phase purity of the colorless phase was checked using XRPD. No significant differences in peak positions and intensities between experimental and calculated patterns were found (Fig. 1). Subsequently, the synchrotron X-ray diffraction study has revealed that colorless crystals correspond to salt **1**. Thus, it was proved that abiraterone acetate can be hydrolyzed in acidic media at presence of iron(III) salt, although no complexation with metal atom occurred. Note also that recrystallization of AbirAc from 2 M and concentrated 48% HBr affords, respectively, starting AbirAc or an amorphous product as obtained from powder X-ray diffraction.

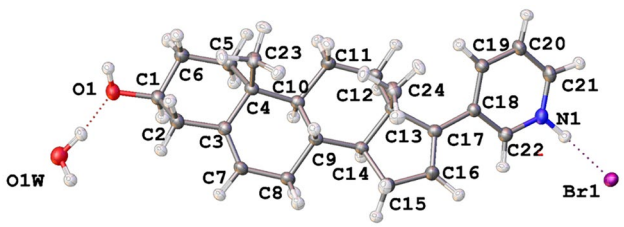

Fig. 2 Molecular view of **1** in representation of atoms with thermal ellipsoids ($p = 50\%$)

Molecular and crystal structure of 1

The unit cell of (HAbirOH)Br · H_2O is represented in Fig. 2. The positions of all hydrogen atoms can be easily revealed from difference Fourier maps and the most expected H-bonds. These should be present for O1…Br1, O1W…Br, and O1W…O1 distances as short as 3.245(2), 3.356(2), and 2.778(3) Å. In addition, the protonation of pyridine fragment is expected from N1…Br1 distance as short as 3.211(2)Å (Table 1). Thus, the positions of all hydrogen atoms were revealed on difference Fourier maps and refined with unfixed bond distances, while ADPs of hydrogen atoms were calculated with SHADE3 web application [18] and fixed at the calculated values as it was previously suggested by Woińska et al. [25]. N1-H1A, O1-H1, and O1W-H

Table 1 H-bond lengths (Å, °) for salt **1**

D—H···*A*	*D*—H	H···*A*	*D*···*A*	*D*—H···*A*
N1—H1A···Br1	1.04(4)	2.16(4)	3.211(2)	178(4)
O1—H1···Br1^{i}	0.93(4)	2.34(4)	3.245(2)	165(3)
O1W—H1WA···O1	1.02(4)	1.77(4)	2.778(3)	172(4)
O1W—H1WB···Br1^{ii}	0.97(3)	2.39(3)	3.356(2)	174(4)
C16—H16···O1W^{iii}	1.09(3)	2.27(3)	3.325(3)	167(3)

Symmetry transformations used: **(i)** $1-x, -1/2+y, 1-z$; **(ii)** $1+x, y, -1+z$; **(iii)** $x, y, 1+z$

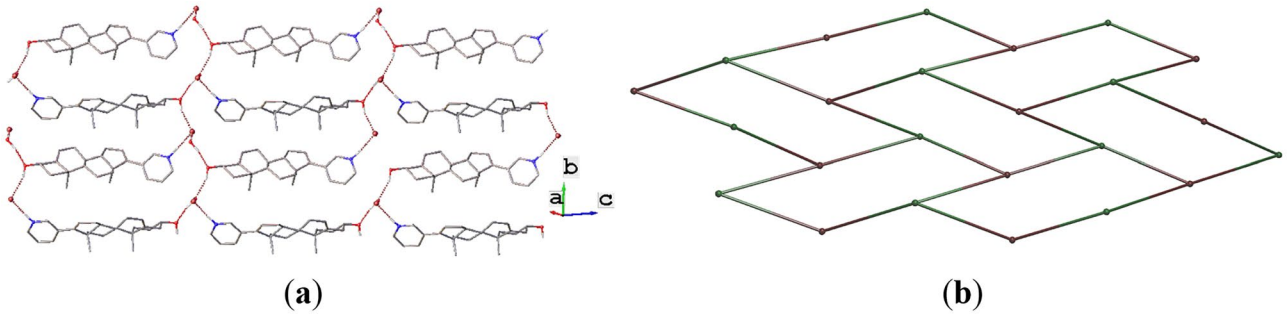

Fig. 3 **a** Fragment of H-bonded layers in (HAbirOH)Br · H_2O, and **b** underlying H-bonded net of salt **1** (centers of cations and anions are depicted as brown and green spheres, respectively, keeping connectivity of the network)

distances (1.04(4), 0.93(4), and 0.97(3)—1.02(4) Å) refined with NoSpherA2 [7] are close to the values obtained from neutron diffraction studies (1.05, 0.98, and 0.97 [26, 27]).

Strong hydrogen bonding in solid **1** results in the formation of H-bonded layers. Parameters of H-bonds are listed in Table 1, and the fragment of the layer is depicted in Fig. 3. The bromide anions and the cations both act as three-connected nodes of the layer (these ions take part in three hydrogen bonds), and water molecules are two-connected nodes or simple linkers (weak C–H…O bonding is not considered). The resulting H-bonded network obtained by simplification of cations, anions, and water molecules to their centers followed by removal of simple linkers as described in Ref. [28] is given in Fig. 3b. It has the honeycomb topology which is one of the most widespread among H-bonded nets of molecular crystals [29].

Packing similarity of 1 and previously reported forms of abiraterone

In several previously reported X-ray studies of solid forms of AbirOH, AbirAc, and $(HAbirOH)^+$, it was shown that the character of intermolecular pairwise interactions is almost independent from the presence of the acetate group or protonation of the pyridine fragment. Particularly, high (up to 82%) contribution of H…H interactions to the Voronoi molecular surface was found [1]. This quantity and the steric repulsion of methyl groups from one another are favorable for retaining the conformation of steroid core unchanged. The crystal packing in salt **1** is very similar to its isostructural chloride-containing analog; both compounds form H-bonded layers (Fig. 4a); moreover, the "Crystal Packing Similarity" tool described in Refs. [30, 31] demonstrates that clusters composed of 20 $HAbirOH^+$ cations in these two salts are also close to each other (Fig. 4a) demonstrating similarity of layers packing through hydrophobic interactions. The role of hydrophobic interactions in packing of abiraterone and its derivatives can be highlighted also by the fact that the "Crystal Packing Similarity" tool also revealed similarly packed chains through H…H interaction molecules in (HAbirOH)Br · H_2O **1** and AbirAc · *p*-HOC_6H_4COOH [2], AbirAc · $HOOC(CH_2)_3COOH$ [2], AbirAc · TAA (TAA = *trans*-aconitic acid [3]), and pure AbirOH (polymorph II [5]; Fig. 4b).

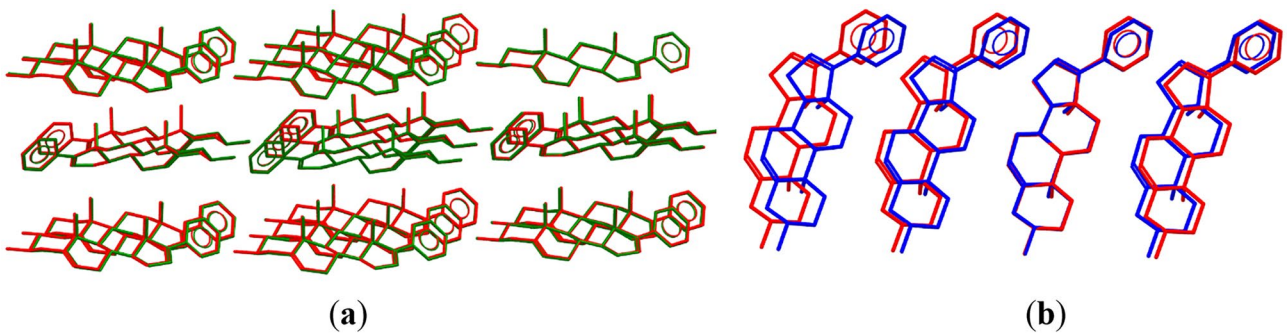

Fig. 4 **a** Comparison of molecular clusters in (HAbirOH)Br · H_2O (red) and (HAbirOH)Cl · H_2O (green); and **b** H…H connected chains in (HAbirOH)Br · H_2O (red) and form II of pure AbirOH (blue)

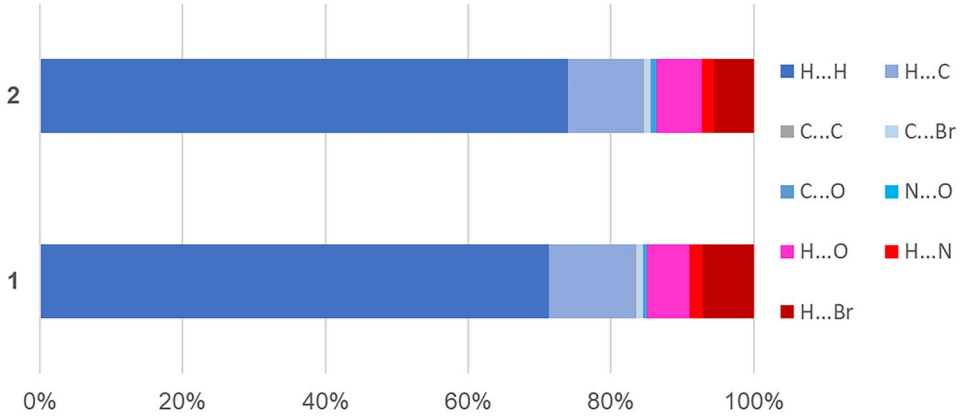

Fig. 5 Contribution of various noncovalent interactions to the molecular Voronoi (**1**) and Hirshfeld (**2**) surfaces

Contribution of various types of interactions to the molecular surface of abiraterone

The molecular Hirshfeld [32] and Voronoi [33] surfaces are well-known approaches for analysis of noncovalent interactions in crystals of molecular compounds. Although these are mainly applied to monomolecular compounds, examples of their application to salts and solvates are also known [1, 34–37]. We performed the analysis of partial contributions of various types of noncovalent interactions to the surrounding of the $HAbirOH^+$ in solid **1** by means of the Voronoi and Hirshfeld molecular surfaces. These approaches give the area of the molecular surface for the cation equal to, respectively, 434.5 and 370.3 $Å^2$. Solid **1** contains atoms of five element; hence, 15 different types of noncovalent interactions can theoretically be found; however, both methods detect nine types only (Fig. 5). Six of them (H…H, H…C, C…C, C…Br, C…O, and N…O) belong to the hydrophobic interactions, and three (H…O, H…N, and H…Br) to hydrophilic, and both approaches indicate that 85% of the molecular surface goes to hydrophobic interactions. This fact is in accord with previously reported data for abiraterone-containing solids [1]. Good correlation between partial contributions of noncovalent interactions to the molecular Voronoi and Hirshfeld surfaces is also typical for molecular solids [38–40]. Difference of molecular volume for two approaches is less pronounced; total volume of the cation is equal to 488.3 and 464.4 $Å^3$ for the Voronoi and Hirshfeld surfaces.

Both surfaces are depicted in Fig. 6. Note that color schemes for the surfaces have different advantages and disadvantages for analysis of noncovalent interactions.

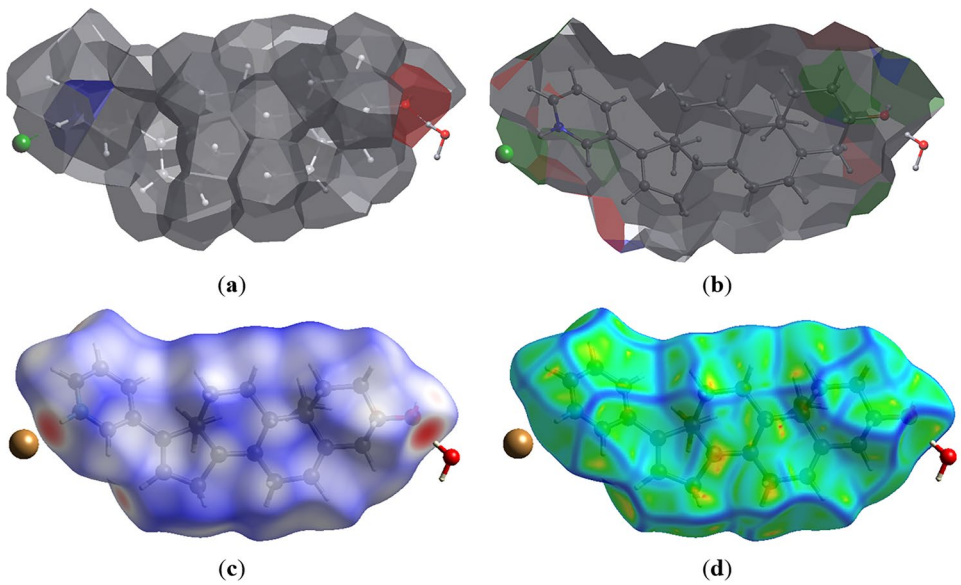

Fig. 6 The molecular Voronoi surface of $HAbirOH^+$ colored in accord with the nature of **a** internal and **b** external atoms (Br, green; C, dark gray; H, gray; N, blue; O, red). The molecular Hirshfeld surface of $HAbirOH^+$ colored in accord with the **c** d_{norm} and **d** curvedness

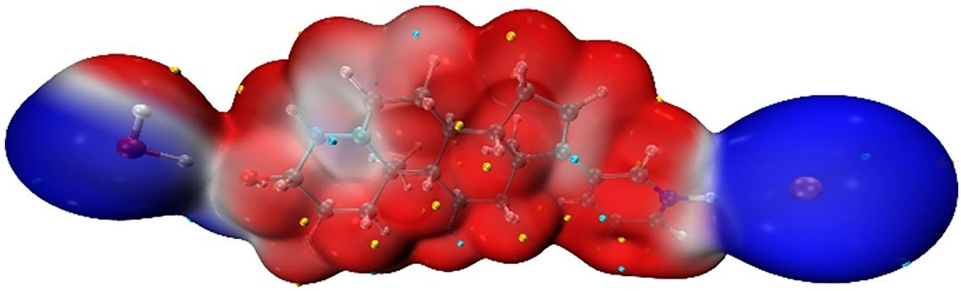

Fig. 7 Electrostatic potential function ranged from – 0.03 a.u. (blue) to 0.03 a.u. (red) mapped on 0.001 isosurface of electron density function

The Voronoi surface allows differentiation between atom types external and internal towards the surface, and gives possibility to extract the surface corresponding towards any pairwise interactions. The Hirshfeld surfaces allow revealing the closest interactions, molecular curvedness, and shape index. Particularly, the N–H…Br bond manifests itself as a red spot on the Hirshfeld surface colored with d_{norm}, and as a region colored with gray and green on the Voronoi surface colored with the nature of an internal and external atoms (Fig. 6a, b, respectively).

Charge density distribution in 1

The wavefunction obtained in NoSpherA2 refinement was utilized to rationalize the information obtained from the analysis of geometry and short contacts. The function of electrostatic potential mapped on 0.001 a.u. demonstrates the character of charge distribution in the unique part of the unit cell of **1**. Bromine atoms, water molecule, hydroxyl group, and double bond C3–C7 appeared to be the regions of negative charge concentration as compared to steroid core that is mostly positively charged (Fig. 7). The comparative analysis of electron density distribution in terms of the QTAIM theory [41] and NCI method [42, 43] has revealed that hydrogen atoms in the steroid core are involved in intramolecular interactions that can be classified as steric repulsion. In most cases, the presence of isosurfaces of RDG function [42, 43] colored by brown and green colors is indicative for steric interactions between hydrogen atoms. Besides, the occurrence of bond critical points (bcps) is also observed (Fig. 8a) for three H…H interactions. Recently, we proposed that bonding H…H interactions can be extracted from all H…H contacts based on atomic Voronoi polyhedra. Particularly, such interactions should be characterized by solid angles Ω of corresponding faces above 10% of full solid angle (4π steradian) [44]. Among 72 faces of atomic Voronoi polyhedra which correspond to intramolecular H…H interactions, only 32 and 5 faces are characterized by Ω > 10 and 15%, respectively. Particularly, the interactions connected by bond paths in Fig. 8a are characterized by Ω = 17, 16, and 16% (Fig. 8b).

Unlike H…H interactions, the N1-H1A…Br1 and O1W-H1WA…O1 have mostly attractive nature. The energies of H1A…Br1 and H1WA…O1 bonds calculated using Espinosa, Mollins, and Lecomte correlation [45] are equal to – 30.2 and – 45.2 kJ/mol that correspond to weak hydrogen bonds. The energies of three H…H interactions are much weaker than hydrogen bonds (5.4–10.1 kJ/mol).

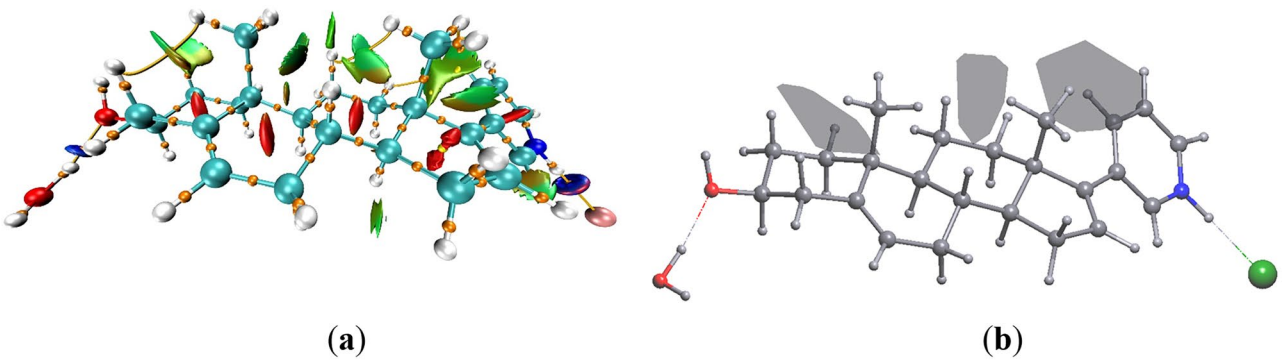

Fig. 8 **a** Molecular graph and RDG isosurface (0.4 a.u.) colored with signλ_2 function and **b** faces of atomic Voronoi polyhedra which correspond to intramolecular H…H interactions (gray). The bcps and bond paths are shown by brown spheres and brown lines, respectively

Conclusions

To sum up, the complexes of abiraterone or abiraterone acetate with Fe(III) salts cannot be easily synthesized in polar media. Hydrolysis of abiraterone acetate to abiraterone and its further protonation was observed instead. The character of crystal packing is governed by combination of O-H…O, O-H…Br, and N-H…Br hydrogen bonds and hydrophobic H…H interactions. The hydrogen bonding between $HAbirOH^+$ and anion or water molecule is too weak to affect molecular conformation. Large molecular surface formed by protons and rigid molecular conformation allow crystallization of H…H connected chains in solids, containing AbirAc, AbirOH, and $HAbirOH^+$. Good correlation of partial contributions of noncovalent interactions to the molecular Voronoi and Hirshfeld surfaces of the cation was observed.

Supplementary Information The online version contains supplementary material available at https://doi.org/10.1007/s11224-023-02210-3.

Acknowledgements The support by the Ministry of Science and Higher Education of the Russian Federation to electronic resources is gratefully acknowledged.

Author contribution A.A.K. and A.V.V. wrote the main manuscript text, P.A.B. prepared the sample and obtained spectral data, P.V.D. collected XRD data and performed an ordinary refinement, A.A.K. performed the NoSphereA2 refinement, and A.V.V. prepared all figures and collected powder XRD data. All authors read and approved the final manuscript.

Funding This research was funded by the Russian Science Foundation, grant number 20-13-00241.

Availability of data and materials CCDC 2222682 contains crystallographic information for this salt and can be obtained from ccdc.cam.ac.uk/structures.

Declarations

Ethical approval Not applicable.

Competing interests A.V.V. declares that she is an Editorial Board Member of Structural Chemistry. The other co-authors declare that they have no competing interests.

References

1. Korlyukov AA, Vologzhanina AV, Trzybinski D, Malinska M, Wozniak K (2020) Charge density analysis of abiraterone acetate. Acta Cryst Sect B 76:1018–1026. https://doi.org/10.1107/S2052520620013244
2. Chennuru R, Devarapalli R, Rengaraj P, Srinivas PL, Dey S, Malla Reddy C (2020) Improving solubility of poorly soluble abiraterone acetate by cocrystal design aided by in silico screening. Cryst Growth Des 20:5018–5030. https://doi.org/10.1021/acs.cgd.0c00153
3. Yang Z, Yang Y, Xia M, Dai W, Zhu B, Mei X (2022) Improving the dissolution behaviors and bioavailability of abiraterone acetate via multicomponent crystal forms. Int J Pharm 614:121460. https://doi.org/10.1016/j.ijpharm.2022.121460
4. Sakai Y, Fukami T, Nagaoka M, Hirosawa K, Ichida H, Sato R, Suzuki K, Nakano M, Nakajima M (2021) Arylacetamide deacetylase as a determinant of the hydrolysis and activation of abiraterone acetate in mice and humans. Life Sci 284:119896. https://doi.org/10.1016/j.lfs.2021.119896
5. Silveira RG, Cunha BN, Tenório JC, de Aguiar DVA, da Cruz SP, Vaz BG, Ellena J, Batista AA, Martins FT (2019) A simple alternative to prodrug: the hydrochloride salt monohydrate of the prostate anticancer drug abiraterone. J Mol Struct 1190:165–170. https://doi.org/10.1016/j.molstruc.2019.04.068
6. Trzcińska K, Łaszcz M, Kuziak K, Stolarczyk EU (2021) Investigating differences and similarities between two new abiraterone polymorphs and its hydrochloride salt monohydrate. J Mol Struct 1225:129124. https://doi.org/10.1016/j.molstruc.2020.129124
7. Kleemiss F, Dolomanov OV, Bodensteiner M, Peyerimhoff N, Midgley L, Bourhis LJ, Genoni A, Malaspina LA, Jayatilaka D, Spencer JL, White F, Grundkötter-Stock B, Steinhauer S, Lentz D, Puschmann H, Grabowsky S (2021) Accurate crystal structures and chemical properties from NoSpherA2. Chem Sci 12:1675–1692. https://doi.org/10.1039/D0SC05526C
8. Aree T, McMonagle CJ, Michalchuk AAL, Chernyshov D (2022) Low-frequency lattice vibrations from atomic displacement parameters of α-FOX-7, a high energy density material. Acta Cryst Sect B 78:376–384. https://doi.org/10.1107/S2052520622002700
9. Hatcher LE, Saunders LK, Coulson BA (2022) Uncovering the role of non-covalent interactions in solid-state photoswitches by non-spherical structure refinements with NoSpherA2. Faraday Discuss. https://doi.org/10.1039/D2FD00158F
10. Vosegaard ES, Thomsen MK, Krause L, Grønbech TBE, Mamakhel A, Takahashi S, Nishbori E, Iversen BB (2022) Synchrotron X-ray electron density analysis of chemical bonding in the graphitic carbon nitride precursor melamine. Chem Eur J 28:e202201295. https://doi.org/10.1002/chem.202201295
11. Saunders LK, Pallipurath AR, Gutmann MJ, Nowell H, Zhang N, Allan DR (2021) A quantum crystallographic approach to short hydrogen bonds. CrystEngComm 23:6180–6190. https://doi.org/10.1039/D1CE00355K
12. Korlyukov AA, Dorovatovskii PV, Vologzhanina AV (2022) N-(4-Methyl-3-((4-(pyridin-3-yl)pyrimidin-2-yl)amino)phenyl)-4-((4-methylpiperazin-1-yl)methyl)benzamide. Molbank 2022:M1461. https://doi.org/10.3390/M1461
13. Lazarenko VA, Dorovatovskii PV, Zubavichus YV, Brulov AS, Koshchienko YV, Vlasenko VG, Khrustalev VN (2017) High-throughput small-molecule crystallography at the 'Belok' beamline of the Kurchatov synchrotron radiation source: transition metal complexes with azomethine ligands as a case study. Crystals 7:325. https://doi.org/10.3390/cryst7110325
14. Svetogorov RD, Dorovatovskii PV, Lazarenko VA (2020) Belok/XSA diffraction beamline for studying crystalline samples at Kurchatov synchrotron radiation source. Cryst Res Technol 55:1900184. https://doi.org/10.1002/crat.201900184
15. Kabsch W (2010) XDS. Acta Cryst Sect D 66:125–132. https://doi.org/10.1107/S0907444909047337
16. Sheldrick GM (2015) SHELXT – integrated space-group and crystal-structure determination. Acta Cryst Sect A 71:3–8. https://doi.org/10.1107/S2053273314026370
17. Sheldrick GM (2015) Crystal structure refinement with SHELXL. Acta Cryst Sect C71:3–8. https://doi.org/10.1107/S2053229614024218
18. Madsen AØ (2006) SHADE web server for estimation of hydrogen anisotropic displacement parameters. J Appl Cryst 39:757–758. https://doi.org/10.1107/S0021889806026379

19. Dolomanov OV, Bourhis LJ, Gildea RJ, Howard JAK, Puschmann H (2009) OLEX2: a complete structure solution, refinement and analysis program. J Appl Cryst 42:339–341. https://doi.org/10.1107/S0021889808042726
20. Blatov VA, Shevchenko AP, Proserpio DM (2014) Applied topological analysis of crystal structures with the program package ToposPro. Cryst Growth Des 14:3576–3586. https://doi.org/10.1021/cg500498k
21. Spackman PR, Turner MJ, McKinnon JJ, Wolff SK, Grimwood DJ, Jayatilaka D, Spackman MA (2021) CrystalExplorer: a program for Hirshfeld surface analysis, visualization and quantitative analysis of molecular crystals. J Appl Cryst 54:1006–1011. https://doi.org/10.1107/S1600576721002910
22. Lu T, Chen F (2012) Multiwfn: a multifunctional wavefunction analyzer. J Compt Chem 33:580–592. https://doi.org/10.1002/jcc.22885
23. Humphrey W, Dalke A, Schulten K (1996) VMD: visual molecular dynamics. J Mol Graph 14:33–38. https://doi.org/10.1016/0263-7855(96)00018-5
24. Goloveshkin AS, Korlyukov AA, Vologzhanina AV (2021) Novel polymorph of favipiravir—an antiviral medication. Pharmaceutics 13:139. https://doi.org/10.3390/pharmaceutics13020139
25. Woińska M, Jayatilaka D, Spackman MA, Edwards AJ, Dominiak PM, Woźniak K, Nishibori E, Sigimoto K, Grabowsky S (2014) Hirshfeld atom refinement for modelling strong hydrogen bonds. Acta Cryst Sect A 70:483–498. https://doi.org/10.1107/S2053273314012443
26. Ceccarelli C, Jeffrey GA, Taylor R (1981) A survey of O-H···O hydrogen bond geometries determined by neutron diffraction. J Mol Struct 70:255–271. https://doi.org/10.1016/0022-2860(81)80112-3
27. Kurki-Suonio K, Merisalo M, Vahvaselkä A, Larsen FK (1976) Neutron diffraction study of nuclear distributions in NH4Cl. Acta Cryst Sect A 32:110–115. https://doi.org/10.1107/S056773947600020X
28. Shevchenko AP, Blatov VA (2021) Simplify to understand: how to elucidate crystal structures? Struct Chem 32:507–519. https://doi.org/10.1007/s11224-020-01724-4
29. Mitina TG, Blatov VA (2013) Topology of 2-periodic coordination networks: toward expert systems in crystal design. Cryst Growth Des 13:1655–1664. https://doi.org/10.1021/cg301873m
30. Childs SL, Wood PA, Rodríguez-Hornedo N, Reddy S, Hardcastle KI (2009) Analysis of 50 crystal structures containing carbamazepine using the *Materials* module of *Mercury CSD*. Cryst Growth Des 9:1869–1888. https://doi.org/10.1021/cg801056c
31. Vologzhanina AV (2019) Intermolecular interactions in functional crystalline materials: from data to knowledge. Crystals 9. https://doi.org/10.3390/cryst9090478
32. A. Spackman M, Jayatilaka D (2009) Hirshfeld surface analysis. CrystEngComm 11:19–32. https://doi.org/10.1039/B818330A
33. Serezhkin VN, Savchenkov AV (2021) Advancing the use of Voronoi-Dirichlet polyhedra to describe interactions in organic molecular crystal structures by the example of galunisertib polymorphs. CrystEngComm 23:562–568. https://doi.org/10.1039/D0CE01535K
34. Almeida CM, de Carvalho JGM, Fujimori M, França EL, Honorio-França AC, Parreira RL, Orenha RP, Gatto CC (2020) Structural investigation of group 10 metal complexes with thiosemicarbazone: crystal structure, mass spectrometry, Hirshfeld surface and in vitro antitumor activity. Struct Chem 31:2093–2103. https://doi.org/10.1007/s11224-020-01564-2
35. Asanbaeva NB, Rychkov DA, Tyapkin PY, Arkhipov SG, Uvarov NF (2021) The unique structure of [(C4H9)4N]3[Pb(NO3)5]—one step forward in understanding transport properties in tetra-n-butylammonium-based solid electrolytes. Struct Chem 32:1261–1267. https://doi.org/10.1007/s11224-021-01732-y
36. Harzallah M, Medimagh M, Issaoui N, Kaminsky W, Ayed B (2023) An original zero-dimensional material: 1, (2-aminoethyl) piperazinuim) tetrabromidomercurate (II) monohydrate, characterization and molecular docking. Struct Chem. https://doi.org/10.1007/s11224-023-02181-5
37. Vologzhanina AV, Ushakov IE, Korlyukov AA (2020) Intermolecular interactions in crystal structures of imatinib-containing compounds. Int J Mol Sci 21:8970. https://doi.org/10.3390/ijms21238970
38. Savchenkov AV, Klepov VV, Vologzhanina AV, Serezhkina LB, Pushkin DV, Serezhkin VN (2014) Trinuclear Sr[UO2L3]2(H2O)4 and pentanuclear {Sr[UO2L3]4}2− uranyl monocarboxylate complexes (L-acetate or n-butyrate ion). CrystEngComm 17:740–746. https://doi.org/10.1039/C4CE02103G
39. Smol'yakov AF, Korlyukov AA, Dolgushin FM, Balagurova EV, Chizhevsky IT, Vologzhanina AV (2015) Studies of multicenter and intermolecular dihydrogen B-H···H–C bonding in [4,8,8′-exo-PPh3Cu-4,8,8′-(μ-H)3-commo-3,3′-Co(1,2–C2B9H9)(1′,2′-C2B9H10)]. Eur J Inorg Chem 2015:5847–5855. https://doi.org/10.1002/ejic.201501029
40. Vologzhanina AV, Kats SV, Penkova LV, Pavlenko VA, Efimov NN, Minin VV, Eremenko IL (2015) Combined analysis of chemical bonding in a CuII dimer using QTAIM, Voronoi tessellation and Hirshfeld surface approaches. Acta Cryst Sect B 71:543–554. https://doi.org/10.1107/S2052520615015279
41. Bader RWF (1990) Atoms in molecules: a quantum theory. Oxford University Press, New York
42. Johnson ER, Keinan S, Mori-Sánchez P, Contreras-Garcia J, Cohen AJ, Yang W (2010) Revealing noncovalent interactions. J Am Chem Soc 132:6498–6506. https://doi.org/10.1021/ja100936w
43. Saleh G, Gatti C, Lo Presti L (2012) Non-covalent interaction via the reduced density gradient: independent atom model vs experimental multipolar electron densities. Compt Theor Chem 998:148–163. https://doi.org/10.1016/j.comptc.2012.07.014
44. Korlyukov AA, Stash AI, Romanenko AR, Trzybiński D, Woźniak K, Vologzhanina A (2023) Ligand-receptor interactions of lamivudine: a view from charge density study and QM/MM calculations. Biomedicines 11:743. https://doi.org/10.3390/biomedicines11030743
45. Espinosa E, Molins E, Lecomte C (1998) Hydrogen bond strengths revealed by topological analyses of experimentally observed electron densities. Chem Phys Lett 285:170–173. https://doi.org/10.1016/S0009-2614(98)00036-0